Addis Ababa University
School of Graduate Studies
Faculty of Science
Department of Earth Sciences

GROUND VELOCITY PREDICTION BASED ON SHOT DISTANCE, SHOT SIZE AND SHOT SITE ENVIRONMENT ACROSS THE MAIN ETHIOPIAN RIFT

A THESIS SUBMITTED TO THE SCHOOL OF GRADUATE STUDIES IN PARTIAL FULFILLMENT OF THE REQUIREMENT FOR THE DEGREE OF MASTER OF SCIENCE, GEOPHYSICS

BY DEMISACHEW ABEBE

JUNE 2005, ADDIS ABABA

Acknowledgement

In the first place in impressed heart fully thanks to the almighty God with out his help and for bivalence , this thesis would have been abandoned long ago .

I would particularly like to give my special respects, and to thank Dr. Tilahun Mammo for his continual support on this thesis and having commented on substantial part of the work. Cheerful thanks also to all my proffesors D.r. Abera Alemu, Dr. Atalay Ayele, Dr. Laeke Marlam, Dr. Tigistu and Dr. Tilahun for their help encouragment and advice which have been most beneficial, and to colleagues in the university and around the country for their help and commitments which have been most constructive.

I would like to acknowledge (1) mekonen Nigatu for his Cooperation for his professional carrier (2) Ato. Melkamu Fentaw for his support and encouragent and to all my companions in Ayssita: Ato . Seid Ahmed, Ato Gebre wolde, Ato Alemseged Yimam and Yonas Gebresilassiee for their favorable assistance

I wish to assert my Gratitude to my in timate friend, rather brother, Fisseha for his patience and support in competing so long till the final manuscript.

I must also thank to my father Ato Abebe Feye, my mom there Bayush, Sisters Senait, Aster and Frezewd and my brother Ermias for their incentive endurance

My final acknowledgment is to my wife Hirut and so Kalab for their support, encouragement and long suffering patience while I have been Closeted with this work and engagement through times of combating with my books

Table of Contents

List of Figures

Abstract

Accurate Prediction of grand velocity is essential in determining seismic shot size which minimizes risk to nearby manmade structures yet still ensures acceptable signal-noise ratio at large distances. In our study ground velocity data from the 2003 EAGLE conducted across the Main Ethiopian Rift were compared with the semi-empirical ORIARD formula on either rare of the MER. The ORIARD formula predicts velocities for scaled distance greater than 1.85 km per kg1/2, but over predicts for velocities less than 1.85 km per kg1/2. However, within MER, the ORIARD formula predicts velocities between 2 and 8 scaled distances, but over predicts velocities of a scaled distance less than 2 km per kg1/2 while under predicts for a scaled distance greater than 8 km per kg1/2.

CHAPTER 1
Introduction

1.1 Location and Geological Setting of the Study Area

The study area is situated across the Main Ethiopian Rift Valley form chefedonsa (8⁰,98'N; 39⁰,12⁰E) to Kula (5⁰,12"N; 39⁰,69'E). As shown in the fig (1) below.

fig(1)

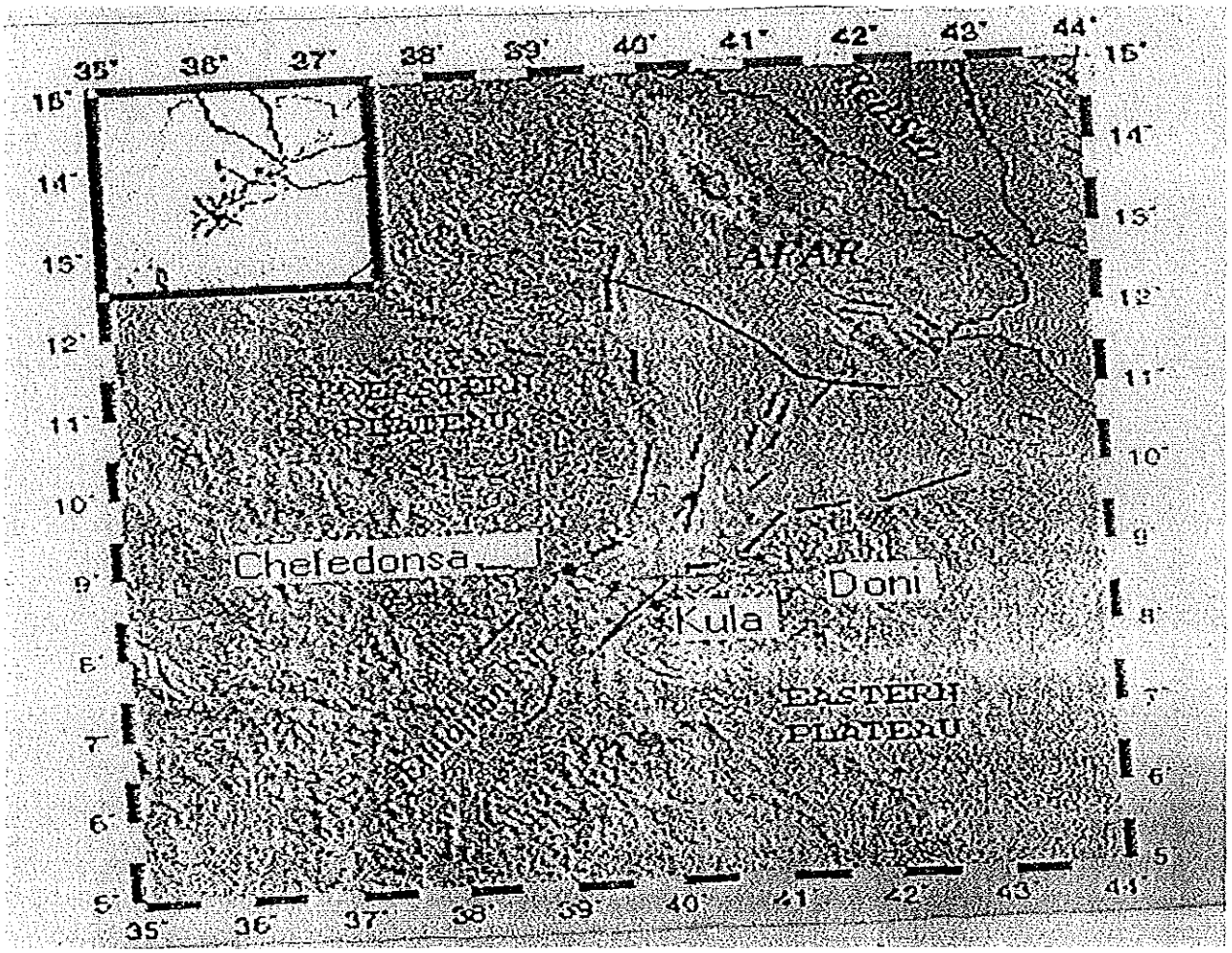

Fig 1 Map of the study area

The main Ethiopian Rift (MER) is the Part of the Great East Africa Rift System, which is one of the major tectonic structure of the Earth and extends for about 6500 km from the middle East (Dead sea-Jordan Valley) in the North to Mozambique in the South. This system consists of three main arms: the Red sea Rift, Afar, Main Ethiopia Rift and the East Africa Rift which develops through Eritrea, Ethiopia, Kenya, Tanzania, Zambia, Malawi and Northern Mozambique floored by a thin continental crust. The East Africa Rift System (EARS) is composed of two rift trends the Eastern and western branches. The western breach develops from Uganda through out lake Tanganyika, where it joins the Eastern branch, following the border between Rwanda and Zaire. The western branch is, however, much less active in terms of tectonics and volcanism although both branches are seismically and tectonically active today (Ethiopian Afar Geo scientific Lithosphere Experiment, 2003). The Red sea and Gulf of Aden are active diverging boundaries along which the Arabian Peninsula is separated from North Africa (fig.2). The three rift systems. Red sea, the Gulf of Aden and the East African systems meet in the Afar depression which is characterized by a shallow tectonically active crust.

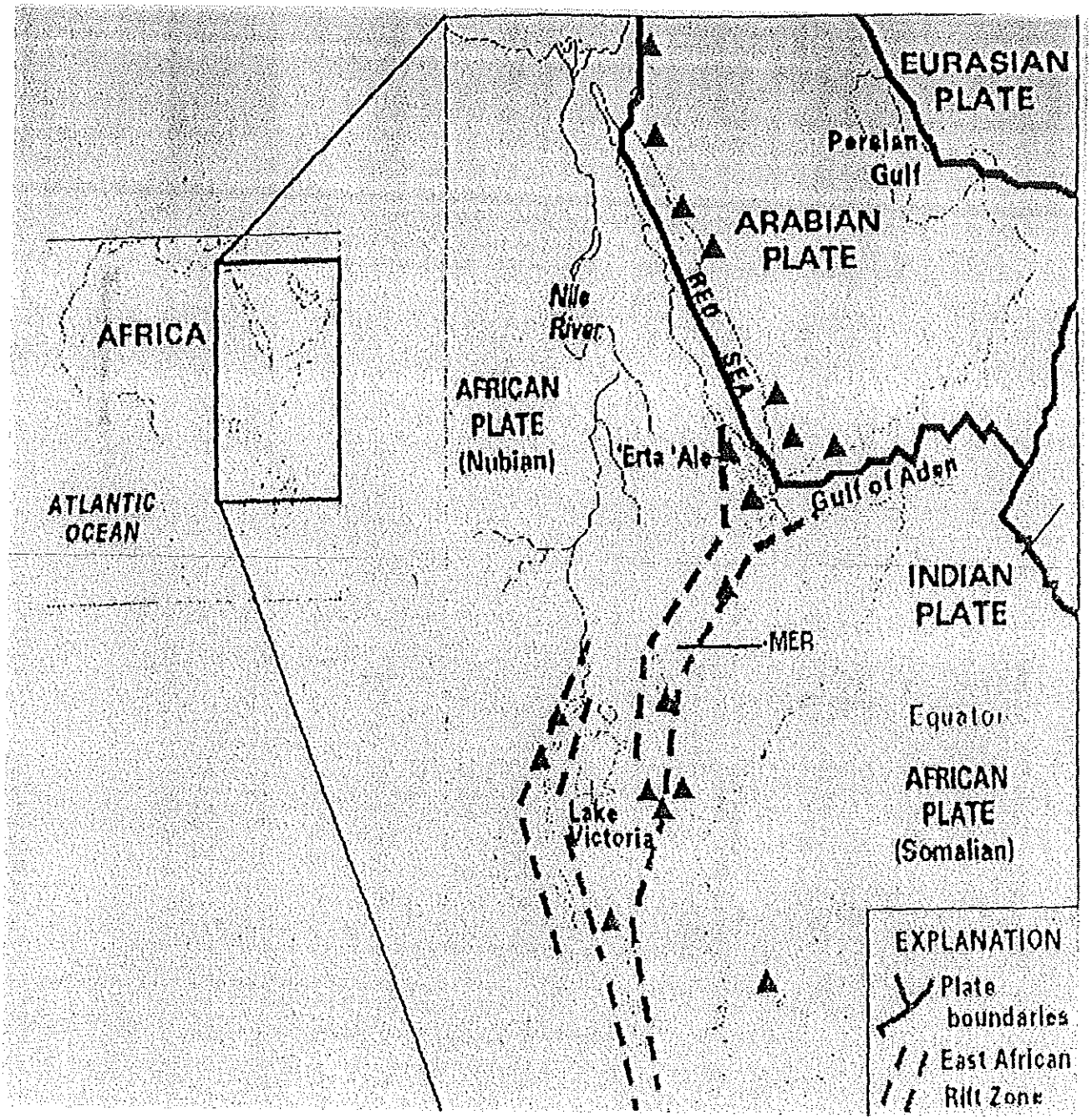

Fig 2 Map of the East African Rift

The Northern Main Ethiopian Rift (MER) develops with in the Paleocene flood basalt province of NE Africa, and forms the youngest arm of the Afar triple junction. High angle, large offset border faults forms after 12 Ma, providing a linkage between the East Africa Rift system and the Southern Red sea Gulf of Aden Rifts (Wolfenden etal., 2004). However, active subsidence migrates to a narrow zone in the central rift by 3.5 ma. Since 1.8 Ma magmatism and faulting has become more localized to is 20 km wide, 60km long ' magmatic segments marked by aligned eruptive centers, fissures and small off set normal faults. This pattern of faulting and magmatism indicates that the East Africa Rift system in Ethiopia is in a stage of development. Further sought the main Ethiopian Rift transects the Ethiopian dome separating the country in to two major blocks the Nubian plate to the west from the Somali plate in the east. This is slowly widening to become oceanic crust with the major geologic feature on the earth, the East African Rift valley. In time the African plate will split apart along the line of the Ethiopian dome and form a new ocean (EAGLE, 2003).

The main Ethiopian Rift which is NNE striking having a width of 10 to 80km extends for about 650 km from the lake Chamo region in the south (4^0,45") to the region of Ayelu volcano in the north (9^0,45") beyond which its NNE trending structure are replaced by the NNW trending structure of the Afar depression with out significant break(Mohr, 1967; Wolde, 1989). the development of the Main Ethiopian Rift is accepted to be due to the drifting apart of the western plateau to the western and the Eastern plateau to the east through tensional faulting .

Eruption of huge volume of volcanicities in the main Ethiopian Rift and Adjacent plateau started in the late Eocene Early Oligocene (Merla etal., 1997; Kazmin etal., 1980; Zanettin, 1993) preceding rift formation. The most important volcanic tectonic in the central sector of the MER occurred in Early Pliocene, with the eruption of voluminous flow of rhyolitic ignimbrites and the collapse of very large calderas (Dipaola, 1972). From the Early Pleistocene to the present tectonic and volcanic activity was concentrated along the Wonj Fault Belt (WFB) and

successively along the Silti-Debrezeit Fault zone (SDFZ) (Mohr, 1962;Di Paola, 1972; Bigazzi et al., 1993). Quaternary volcanism, faulting, tensional fissures on a hard rock, earthquake catalogue of he region and geodetically measure extension rate have been the main indicators of the tectonic activity in the East Africa Rift. The seismcity studies in Ethiopia and the adjacent area confirm that this fault system is still developing. Most of the rocks exposed along the Ethiopian rift is mainly covered by Quaternary basaltic, trachytic and rhyolitic lavas, pyroclastics flow and fall deposits, and volcanic elastics sediments (korme, 1997). The WFB comprises three en-echelon, NNE-trending segments with in the lakes basin (Mohr, 1960, Lioyd, 1977) named from south to North the Corbetti-Shalla, Shalla-Ziway and East Ziway segments.

Moho depths vary from 25 to 31 km with in the main Ethiopian Rift (MER) and Afar Depression, and the crust is characterized by high poisons ratio of 0.30-0.36. Beneath westerns and eastern plateau on either side of the Main Ethiopian Rift, crystal thickness ranges from 33 to 44 km, and Poisson's ratio varies from 0.23 to 0.28 (EAGLE, 2004) typical for Precambrian crust. These results suggest that Cenozoic rifting and volcanism, where as the Precambrian crust beneath the rifted regions has been dramatically thinned in some places and compositionally altered by the addition of mafficrocks, have not significantly modified the Precambrian crystal structure beneath the Ethiopian plateau. The high poisons ratio for the MER and Afar crust suggests that the partial meets are also present in the crust. (EAGLE, 2004).

The central sector of the MER consists the five large lakes of tectonic or volcano tectonic origins. These are Ziway, Langano, Abyata, Shala and Awassa lakes MER and its shoulder are made of silicic phyroclastic materials (Mohr, 1962, Dipaola, 1972), they are early middle Pliocene (Woldegebriel et al, 1972). The thick section of rhyolites, ignimbrites interlaid with basalts and unwelded tuffs and ash flows and thrachytes commonly named as Nazret Groups form the large part of the rift floor and out crops in some parts of the rift and escarpments and the adjacent

plateau margins (Kazmin, 1978) where as large area of the rift floor covered by volcanic lacustrine and fluvial lacustrine deposits (Benvenuti and Balewald, 2002). Along the eastern margin f the rift the Alafi basalt are conformably over lapped by a unit of flood basalts and siliceous rocks which in turn over lapped with slight un conformity by silicic volcanics of the Nazret Group (Kazmin and Berhe , 1978).

In the MER Aden series basalts are rather rare the most notable occurrence is northwest of lake Margarita, east of lake ziway, and, along the foot of the Gouraghe host extending northwards. Pleistocene silicic lavas and ignimbrites are significantly restricted to WFB of the rift system (Mohr, 1967)

The floor of the rift rises about 600m from north to south, reaching maximums elevation of 1800m in the Meki water shed. Fragmentation of the rift floor formed the youngest structural deformation largely concentrated in a narrow 5-12 km wide belt of normal faults, known as the Wonji Fault Belt. (Mohr et al.) 1980; Lloyd, 1977) the WFB has a NNE orientation along the rift margin envelope (Mohr, 1980) Pleistocene silicic lavas and ignimbrites are significantly restricted to the Wonji Fault Belt to the rift system. The silicic centers occur as fairly large cones frequently manifesting simple or compound calderas. The cones are composed of silicic lavas, ignimbrites and pumice flows (Gibson, 1967b, Mohr, 1962b, 1966b). Some of the latest lavas of the WFB silicic are of Holocene age, in particular associated with calderas of Fentale (Mohr, 1967).

1.2 Lithotomical Units of The Study Area

1.2.1 Intra rift complex.

The upper Miocene Quaternary products constitute the floor of the main rift and its successive filling is taken as rift complex.

The first group of this complex forming the floor of the rift is the Nazret group. The lithologic units of the Nazret group are ignimbrite with fiamme, pumice, ash and rhyolite flows in the MER margins and adjacent plateaus. (Kazmin and Berhe, 1978). In the rift floor its thickness is 200-250m and tends to thin out on the escarpments. In composition the ignimbrites are sub alkaline rhyolite and trachytes with rare per alkaline varieties. This unit comprises also rhyolite and trachytes domes (Gara Bokan, Dikub), which are different formation with age ranging from about 7 to 3 Ma. (Mohr, 1971; Zanettin and Justine Visentin, 1974).

The other unit which outcrop along the border of the central plain to the Chofedonsa unit (Mazzarini, 1999). It consists of fall deposits and poorly welded ignimbrites of rhyolitic composition. The Chefedonsa unit rests upon the Addis Ababa basalt and lacusterine deposit in the south western and covered by the Nazret group in the eastern and Northeastern areas. The total thickness of the unit varies from few meters to 40m close to Chefedonsa village, where the most complete section exposed. Fission track analysis in a section close to Chefedonsa village yielded an age of 2.2 Ma (Mazzarini 1999).

1.2.2 Rift Axis Complex.

It includes the Quaternary Holocene sequence of the young central volcanoes, lacusterine deposits and basaltic cinder and spatter cones. This sequence presents the some volcanic and structural features recognized in the younger sequence of the adjacent MER (Kazmin and Berhe 1978). the different units in this complex are:-

Zikwala volcanic unit:- this unit is an isolated well preserved composite cone. Lavas are the dominant product, with pyroclastic mainly occurring at the foot of the volcano. The lavas of this unit are composed of per alkaline trachytes, which are generally anorthoclase phyric. Radiometric ages range from 1-3 Ma to 0.85 ma.

Bishoftu volcanic unit:- This unit forms a NNE trending belt outcropping mainly in the eastern flat area of Debrezeyt. It is also known as Wonji basalt. The two groups of this unit are the spatter and cinder cones with associated tabular lavas and phreatomagmatic deposit. The latter consisting mainly of surges and highly fragmented deposits with maars and tuff rings.

Bofa Basalt:- Bofa basalt are well developed in the northern and central part of the MER. The lower age limit of 3.5 Ma has been reported by Kazmin etal. 1980b. this basalt is olivine, mostly aphyric Pliocene flood basalt known by different names in different localities, Wolenchiti basalt (Meyer etal., 1975), Bishoftu basalt and rhyolities (Zanettin and Justin, 1994) and rift floor basalt (U.N. geothermal project, 1972).

1.3 The Cross Rift Lineaments

The MER in particular shows isolated cross-rift lineaments as a separating line (Mohr, 1967). The displacements of the plateau-rift margins are along the cross rift lineaments of the Ethiopian rift system. The cross-rift lineament trend WNW-ESE in the MER that are remarkable for their linearity and their persistence over long distances.

The dense swarms of NNE-SSW trending steep normal faults, still active on the margins along the Silti-Debrezeit Fault Zone (SDFZ) on the West and the Wonji Fault Belt (WFB) on the east accommodate total offsets of the rift floor and the plateaus (Di Paola, 1972, Woldegebriel etal. 1990). WFB at the floor of the MER is marked by persistent belt of intense, fresh faulting has dextral displacement. The faults are short and normal types and are notably associated with tensional fissures (Gibson, 1967b) the WFB is frequently, but not always, axial to the rift and is dextrally displaced along the same cross-rift lineaments that displaced the

rift margins. It is a line along which recent lavas aid ignimbrites have erupted, and the whole tectonic association of the crustal tension along the rift (Mohr, 1967a). The silicic centers of the WFB are situated where there is an intersection from cross-rift lineaments and their calderas or craters are elongated in the direction of the cross lineament.

The ESE-WNW Yerer volcanic line marks a faulted and possibly wrapped boundary between the plateau rocks to the north and the rift ignimbrites to the south. Moat scarps can be seen to be major structural down wards in place, most can be seen to be structural down warps commonly modified by faulting where as the structure of the directly opposing rift margin near Asela is dominated by normal faulting (Mohr, 1966); with in the rift Quaternary tensional fault is dominant.

CHAPTER 2

2.1 Theory

The propagation of a disturbance though a material medium is mechanical move. The mechanical wave (Seismic wave), which consists of tiny packets of elastic strain energy, is produced by a great variety of physical phenomena including walking, running ears, hammering, explosive and natural service event. Seismic surveys use sensors (geophone) to defect signals. They are used to convert seismic energy in to a measurable voltage.

2.1.1 Stress

When an external force F is applied across an area A of a surface of a body, forces inside the body are established in proportion to the external force. The ratio of the force to area (F/A) is known as stress.

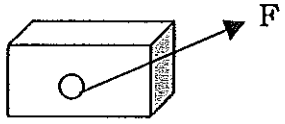

Fig. 2-1 force acting at a point.

Stress can be resolved in to two components, one at right- angle to the surface (normal or dilatational stress) and one in the plane of the surface (shear stress).

Since the force F shown in fig. 2-1 is a vector quantity, it can be resolved in to thee component F_{x_1} F_{y_1} F_Z. In the same manner the area A of the body up on which the force F applied can also be resolved in to three components A_X, A_Y, A_Z. Then the nine components of stress are computed as follows.

$$X_x = \frac{F_x}{A_x} \qquad X_y = \frac{F_y}{A_x} \qquad X_z = \frac{F_z}{A_x}$$

$$Y_x = \frac{F_x}{A_y} \qquad Y_y = \frac{F_y}{A_y} \qquad Y_z = \frac{F_z}{A_y} \text{ ---------- (1)}$$

$$Z_x = \frac{F_x}{A_z} \qquad Z_y = \frac{F_y}{A_z} \qquad Z_z = \frac{F_z}{A_z}$$

If you consider a small cube with forces at right angle to the axes, the cube will be out of equilibrium and to tated unless $X_y = Y_x$, $X_z=Z_X$, $Y_z=Z_y$. Thus there are really six different component of stress. The stress components X_y, Y_y and Z_z are called principal stress which are either tensions or compressions. The remaining components of stress X_y, X_z and Y_z are called shear stress.

2.1.2 Strain

The stressed body under goes strain, which is the amount of deformation expressed as the ratio of the change in length (or volume) to the original length (or volume).

Consider two neighboring particles of the solid at position x,y,z and x+dx, y+dz. As the body deforms, they will be displace by amounts u,v,w and u+du, v+dv, w+dw. If du,dv,dw are zero, so that the two particles move together, there is no resulting strain, and consequently no restoring stress. Hence the strain will depend on the partial derivative of u,v,w with respect to x,y,z. There are nine such derivatives. However, mathematical analysis shows that actual deforming strain depends on only six different combinations of derivatives.

The six components of strain are ordinarily defined as

$$e_{xx} = \frac{\partial u}{\partial x} \qquad e_{xy} = \frac{\partial v}{\partial x} + \frac{\partial u}{\partial y}$$

$$e_{yy} = \frac{\partial x}{\partial y} \qquad e_{xz} = \frac{\partial w}{\partial x} + \frac{\partial u}{\partial t} \text{ ----------(2)}$$

$$e_{zz} = \frac{\partial w}{\partial z}$$

$$e_{yz} = \frac{\partial w}{\partial y} + \frac{\partial x}{\partial y}$$

Given any condition of strain, it is always possible to choose the axes so that any one point $e_{xy} = e_{xz} = e_{yz} = 0$. These axes are the principal axes of strain of that point, and the remaining components e_{xx}, e_{yy}, e_{zz} are the principal strain.

2.1.3 Relation of Stress to Strain

Generalization of Hook's Law

Stress and strain are related since one depend on the other. To define the equation of motion by strain components we have to relates stress and strain by some generalization of Hook's law. With six components of each, the generalization is not unique and we start with assumption that the relation between stress and strain linear equation. Since any component of stress may depend on all six components of strain, we would have

$$X_x = Ae_{xx} + Be_{xy} + Ce_{xz} + De_{yy} + Ee_{yz} + Fe_{zz} \text{ ---------- (3)}$$

And five similar equations for the other components of stress. The coefficients A,B,D,E,F, etc, would be number characteristics of the particular solid, specifying its elastic properties the six equations would thus give 36 elastic coefficients.

However, seismology chiefly uses the result of an Isotropic medium when 36 elastic parameters reduce to 2.

The choice of the principal coefficients may be made in a variety of ways, giving different forms to the equation of motion. According to Richter, 1957, the most important choice is that made by Lame. Denoting his two elastic coefficients by λ and μ, the stress-strain equation for an Isotropic solid can be written as

$$X_x = \lambda\theta + 2\mu e_{xx} \qquad x_y = \mu e_{xy}$$
$$Y_y = \lambda\theta + 2\mu e_{yy} \qquad X_z = \mu e_{xz} \text{ ---------- (4)}$$
$$Z_z = \lambda\theta + 2\mu e_{zz} \qquad Y_z = \mu e_{yz}$$

2.1.4 Coefficients of Elasticity

Of the two Lame constants introduced in the preceding section, μ has a relatively simple physical significance. It measures the resistance of elastic body to shearing deformation and is termed the modulus of rigidity. Its value can be determined directly by experiments. Other elastic constant may be expressed interms of these by applying the equation of their definitions.

Place the medium under uniform hydrostatic compression so that $X_x=Y_y=Z_z$ and $X_y=X_z=Y_z=0$. The equation then becomes.

$T = \lambda\theta + 2\mu e_{xx}$

$T = \lambda\theta + 2\mu e_{yy}$

$T = \lambda\theta + 2\mu e_{zz}$

Adding and applying the definition of θ, we find.

$K = P/\theta = \lambda + 2\mu/3$ 5a

We define K as the bulk modulus, or modulus of incompressibility.

Next take a rod of square cross-section extending parallel to the X- axis and subjected only to pressure or tension applied perpendicular to the ends.

Assuming equilibrium the stress and strain are uniform throughout the rod. We may put $X_x = T$ and set the other stress components equal to Zero.

Than $T = \lambda\theta + 2\mu e_{xx} = (\lambda+2\mu)\, e_{xx} + \lambda\,(e_{yy}+e_{zz})$ ---------- a

$O = \lambda\theta + 2\mu e_{yy} = (\lambda+2\mu)\, e_{xx} + \lambda\,(e_{xx}+e_{zz})$ ---------- b

$O = \lambda\theta + 2\mu e_{zz} = (\lambda+2\mu)\, e_{zz} + \lambda\,(e_{xx}+e_{yy})$ ---------- c

and $O = e_{xy} = e_{xz} = e_{yz}$ ---------- d

Equations (b) and (c) together require that $e_{yy} = e_{zz}$ from either we then find Poisson's ratio:

$$\rho = -\frac{e_{yy}}{e_{xx}} = \frac{\lambda}{2\lambda+2\mu} \quad \text{---------- 5b}$$

Subtracting (b) from (a)

$T = 2\mu\,(e_{xx} - e_{yy})$

Defining young's Modulus E as T/e_{xx} we arrive at

$E = 2\mu\,(1+\rho)$ ---------- (5c)

Young's modulus (E) measures the resulting elongation, while Poisson's ratio (ρ) measures the accompanying decrease in cross- section relative to extension.

Any two of the elastic coefficients named in this section are sufficient to define the properties of an ideal isotropic elastic solid.

2.1.5 Reduced Equation of Motion Elastic Waves

When the force of applied on a deformable body is equal to zero the particles in the body as well as the body itself will be set in motion. The motion of the particles of the body is governed by the equation called wave equation.

Let a small volume of mean density σ be displaced from equilibrium position, so that u, v,w are the components of the displacement vector. The components of its acceleration of the second derivatives of u, v,w with respect to time. The force acting parallel to the axis of x is determined by the derivatives of the three components of stress X_x, X_y, X_z which represent forces acting in that direction, in such away that the Newtonian equation of motion takes the

$$\rho \frac{\partial^2 u}{\partial t^2} = \frac{\partial X_x}{\partial x} + \frac{\partial X_y}{\partial y} + \frac{\partial x_z}{\partial z} \text{----------6}$$

With two analogous equation for the force parallel to Y and Z. The next step is to take expressions for the stress components in terms of the strain components and elastic components and substitute these in to the equations of motions of equation (b)

$$\rho\, \partial^2 u = \lambda \frac{\partial \theta}{\partial x} + \partial\mu \frac{\partial}{\partial x}\frac{(\partial u)}{\partial x} + \frac{\partial}{\partial y}\mu \frac{(\partial v}{\partial x} + \frac{\partial u)}{\partial y} + \frac{\partial}{\partial t}\mu \frac{(\partial w}{\partial x} + \frac{\partial u)}{\partial z}$$

$$= \lambda \frac{\partial^2 u}{\partial x^2} + \lambda \frac{\partial}{\partial x}(\partial v/\partial y) + \lambda \frac{\partial}{\partial x \partial t}(\partial w) + \frac{2\mu \partial^2 u}{\partial x^2} + \mu \frac{\partial}{\partial x \partial y}(\partial v) + \mu \frac{\partial^2 u}{\partial y^2} + \mu \frac{\partial}{\partial x \partial z}(\partial w) + \mu \frac{\partial^2 u}{\partial t^2}$$

$$= \lambda \frac{\partial}{\partial x}\frac{(\partial u}{\partial x} + \frac{\partial v}{\partial y} + \frac{\partial w)}{\partial t} + \mu \frac{\partial}{\partial x \partial x}(\partial u + \frac{\partial v}{\partial y} + \frac{\partial w)}{\partial t} + \mu \frac{(\partial^2 u}{\partial x^2} + \frac{\partial^2 u}{\partial y^2} + \frac{\partial^2 u)}{\partial t^2}$$

$$= \lambda \frac{\partial \theta}{\partial x} + \mu \frac{\partial \theta}{\partial x} + \mu \Delta^2 u.$$

$$\therefore \rho \frac{\partial^2 u}{\partial t^2} = (\lambda+\mu) \frac{\partial \theta}{\partial x} + \mu \Delta^2 u.$$

and for the other two equation of motions, the equation of motion then take the standard form.

$$\rho \frac{\partial^2 u}{\partial t^2} = (\lambda+\mu) \frac{\partial \theta}{\partial x} + \mu \Delta^2 u \text{ ---------- (6a)}$$

$$\rho \frac{\partial^2 v}{\partial t^2} = (\lambda+\mu) \frac{\partial \theta}{\partial y} + \mu \Delta^2 v \text{ ---------- (6b)}$$

$$\rho \frac{\partial^2 w}{\partial t^2} = (\lambda+\mu) \frac{\partial \theta}{\partial t} + \mu \Delta^2 w \text{----------(6c)}$$

If one takes the partial derivatives of equation (ba), (6b), (6c) with respect to x,y,z respectively, the result is

$$\rho \frac{\partial^2}{\partial t^2} \left(\frac{\partial v}{\partial x}\right) = (\lambda+\mu) \frac{\partial^2 \theta}{\partial x^2} + \mu \Delta^2 \left(\frac{\partial u}{\partial x}\right) \text{---------- (7a)}$$

$$\rho \frac{\partial^2}{\partial t^2} \left(\frac{\partial v}{\partial y}\right) = (\lambda+\mu) \frac{\partial^2 \theta}{\partial y^2} + \mu \Delta^2 \left(\frac{\partial v}{\partial y}\right) \text{----------(7b)}$$

$$\rho \frac{\partial^2}{\partial t^2} \left(\frac{\partial w}{\partial z}\right) = (\lambda+\mu) \frac{\partial^2 \theta}{\partial t^2} + \mu \Delta^2 \left(\frac{\partial w}{\partial z}\right) \text{----------(7c)}$$

then adding equation (7a), (7b), (7c) we get

$$\rho \frac{\partial^2 \theta}{\partial t^2} (\lambda+\partial\mu) \Delta^2\theta \text{---------- (8)}$$

If one forms the derivative of (6a) with respect to y and subtracts from it the derivative of (6b) with respect to x1 the first terms on the right disappear, giving

$$\rho \frac{\partial}{\partial t^2} (\partial u/\partial y - \partial v/\partial x) = \mu \Delta^2 \left(\frac{\partial u}{\partial y} - \frac{\partial v}{\partial x}\right) \text{---------- (9a)}$$

and, by the other two analogous operations on pairs (6)

$$\rho \frac{\partial^2}{\partial t^2} \left(\frac{\partial u}{\partial t} - \frac{\partial w}{\partial x}\right) = \mu \Delta^2 \left(\frac{\partial u}{\partial t} - \frac{\partial w}{\partial x}\right) \text{---------- (9b)}$$

$$\rho \frac{\partial^2}{\partial t^2}\left(\frac{\partial v}{\partial t} - \frac{\partial w}{\partial y}\right) = \mu\Delta^2\left(\frac{\partial v}{\partial t} - \frac{\partial w}{\partial x}\right) \text{----------(9c)}$$

Equation (8) is a scalar wave equation; (9a), (9b), (9c) are the three components of a vector equation. In (8) the wave velocity is given by $C^2 = (\lambda+2\mu)/\rho$ and in (9) by $C^2 = \mu/\rho$

2.2 Types of Seismic waves

2.2.1 Body waves

In the previous section it is shown there are two simple methods of combining derivatives of the three equation of motion in to an equation or a set of equation of the form of the wave equation.

Equation (8), in fact, represents wave propagation of the quantity θ, which is a cubical dilation; it is a compressional or rarefactional waves. These types of waves are designated by p and the vibration is longitudinal to the direction of prorogation along the ray.

The vector quantity which appears as the wave parameter in Equation (9) is known as the curl of the displacement vector whose components are u, v, w. waves of this type can exist only in solids. The vibration is transverse; at right angle to the ray such waves are called shear waves (s waves).

Both s and p waves pass through bulk of the medium and are known as body waves.

2.2.2 Surface waves

Theory shows that only P and S type of wave can exist in an ideally elastic isotropic and homogenous solid of infinite extent. However, theory also shows that as soon as boundaries or discontinuities exist, waves of other types may arise and are called surface waves.

Surface waves travel along the outer surface layer of rocks. They do not penetrate in to rock mass. The wave motion of surface wave decreases with depth. Surface waves are larger than body waves but travel slower (frequency). These waves are the waves which causes most of the vibration problem and complaints. Surface waves are also the large energy carriers and produce the largest motion. There are two basic types of surface waves. These are:

Love wave:- love waves are transverse waves that propagate in a surface layer on top of another medium (soil overlying rock).

Raleigh wave:- Raleigh waves travel in the free surface and the particle motion is elliptical.

CHAPTER -3

Blast induced ground vibration

3.1 Chemical Explosive as the source of seismic wave.

Blasting operation is equivalent to the application of transient forces to certain medium in which seismic wave is produced. Here a bore hole is drilled in to the rock in which explosive materials are buried when explosives are detonated in blast hale, the chemical reaction of the explosive produce a high pressure gas need large volume to occupy which is much greater the original volume. As a result this gas pressure (detonation pressure) crushes the rock adjacent to the blast hole. The detonation pressure decays or dissipates quickly. The second phase which immediately follows or in conjunction with the detonation phase is the shock or stress wave propagation phase. When the wave front moves forward, it will encounter discontinuities and/or interfaces At these points, some energy is transferred and some is reflected back.

During and after the stress wave propagation, high pressure, high temperature gas extends radial cracks and any discontinuity fracture, joint. The explosive energy will always take the path of the least resistance. Once the blasted rock is separated from the bedrock, no further fracturing occurs because the gas pressure escapes. This entire process occurs with in a few milliseconds from detonation of the explosives.

In basic terms, when an explosive buried in the ground is detonated part of the energy is spent in crushing the rock, part of it transmitted through the earth in the form of waves or vibration and some waves will escape in the form of noise to

the air. These waves cause neither ground motion nor significant damage to any structure.

3.2 TERMINOLOGY AND COMPONENTS OF GROUND VIBRATION

Vibration is the wave motion created from an energy source. Primarily, blast induced ground vibration is the result of the detonation pressure pushing the blasted rock away from the bedrock. This large force against the bedrock or unbroken portion causes the bedrock to vibrate. When the vibration is transmitted through the ground, this is called propagation. The propagation velocity is the speed at which the propagation wave travel. As the vibration is reduced or decays, this is called seismic attenuation.

The ground vibration caused from blasting is similar to the motion of a floating object placed in the water near the energy source. The distance between the wave crests that moves the object is the wavelength.

The speed at which they move out ward from the energy source and past the object is the propagation velocity.

The particle velocity is the speed at which the object bops up and down, and the frequency is the number of times the object bops up and down in one second.

In blasting, the ground particles oscillate in responding to a vibration wave. This oscillates is measured in particle velocity. The maximum rate is the peak particle velocity (PPV).

Particle motion is defined as ground particles oscillation in response to the arrival of the vibration wave, basically body waves and surface waves.

Frequency is the number of time the particles move back and forth in one second. This back and forth motion can also referred to as oscillation. The number of Oscillations/second or cycles /second that a particle makes under the influence from the vibration wave is measured in Hertz (Hz).

Also the term acceleration may be used to define the vibration wave peak or intensity. Acceleration should always be examined in terms of the principal frequency and should not be used as a stand- alone limit. Acceleration is defined as the velocity per unit time.

The combination of vibration wave peak velocity (the peak speed the particles moves from rest to the highest displacement and back down and the frequency (number of movements in one second) are used to calculate acceleration. The gravitational acceleration on the earth's surface (constant of 386.4inches/second= 1gravity(g) is used to convert the acceleration measurement (which is measured in inches/second^2) to gravity.

Where units of acceleration= gravity, V=PPV (ips),f=frequency

The formula used to approximate maximum acceleration is

$$Accel=2\pi vf/386.4$$

3.3 vibration predication formulas

Basic vibration prediction incorporates the use of scaled distance.

3.3.1 Scaled Distance

Scaled Distance (SD) is scaling factor that relates similar blast effects from various charge weights of the same explosive at various distance. Scaled distance is calculated by dividing the distance of the seismograph of concern by a fractional power of the weight of the explosive material.

There are two type of accepted scaled distance formulas used in blasting, square root scaling and cube root scaling.

Square Root Scaling

Square root scaling is the general formula used in most construction-blasting regulation and general blasting situations, where the charge can be considered linear. This is useful as a beginning estimate for vibration control and provides a conservative and safe charge weight for the test blast program. Since explosive confinement is not taken into consideration, there can and usually is a large vibration in results.

Cube root scaling

Cube root scaling is used for blasting in the extreme near field where the charge can be considered a point charge or in explosions involving very large quantities such as those created by nuclear explosions.

Ambraseys and Hendron suggested cube root scaling for use in predication of blast vibration in the year 1968.

Square Root Scaled Distance formula

Scaled Distance (SD)=Distance Seismograph/(weight) $^{1/2}$

Or

Weight = $(D/SD)^{1/2}$

Cube Root Scaled Distance formula

Scaled Distance (SD)= Distance Seismograph/(weight)$^{1/3}$

OR

Weight=(D/SD)^3

Delay regulations usually states that only a certain amount of expositive may be detonated per delay, this has come to be known as the 8 millisecond delay window or 8ms window. What this means is that amount of explosive being detonated at a given time not overlap with other blast holes being detonated with in 8ms.Years ago, researchers realized that the charges needed to be separated to achieve optimum fragmentation and vibration response. At the time, the explosive initiation systems available could provide a separation of at least 8ms on paper, so 8ms was recommended as the minimum time needed for separation of charges.

3.3.2 Vibration Prediction

Basic prediction of peak particle velocity can be achieved using Oriards formula, which follows:

$PPV = k \times (D/W^{1/2})^{-1.54} = k \times (SD)^{-1.54}$

Where PPV – is the peak particle velocity

SD - scaled distance

k- confinement factor

Lower bound =20

Upper bound=184

3.3.3 Vibration Predication with Hendron's Formula and Cube Root Scaling

Using the formula $PPV = k\ (D/W^{1/3})^{-1.54}$ vibration for very close-in or tight blast can be predicated in the same format as using oriard's formula except substituting cube root scaled distance factor for the square root scaled distance factor.

To predict vibration and check the out put information recorded by seismographs in a seismograph array; both formulas can be used to determine the correctness of data.

When setting up a seismograph array, seismographs are setup at the closest point of concern to the blast. In tight blasting situations, this can lead to erroneous data. To validate data, other seismographs should be set up in-line and behind the closest unit.

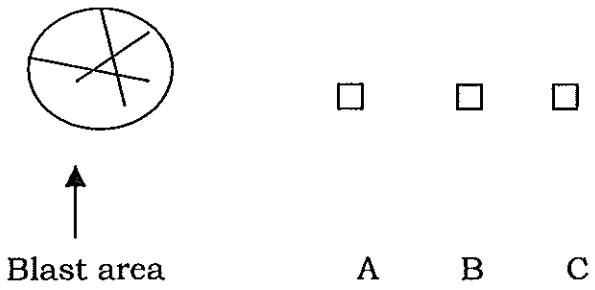

Fig.4 a typical seismograph array.

A B and C are seismographs, arranged in-line from the blast, since seismograph A is placed closest to the blast in tight blasting situation, it can lead erroneous data.

To avoid this we calculate the expected peak particle velocity for seismograph A and compare the data using the following steps.

determine the distance of seismograph: A

determine the distance of seismograph: B

determine the distance of seismograph: C

read the PPV of seismograph: A

read the PPV of seismograph: B

read the PPV of seismograph: C

take-charge wt

Determine the scaled distance of A,B and C

Determine the k factor for seis B from its scaled distance and PPV

Determine the k factor fro seis C from its scaled distance and PPV

Take the average of the two k factors $=(k_B + k_C)/2= k_{av}$

finally, calculate the expected peak particle velocity for seismograph A and compare the data.

3.4 Purpose of the study

1.To investigate ground particle velocity variation with distance, shot weight and shot site environment.

2.To determine the confinement factor.

3.To confirm whether the ORIARD formula was an appropriate predictor of ground velocity and thus acceptable shot size

3.5 Methodology

A. Controlled source released seismic wave data will be taken by geophone arrangement with inter-geophone dispersion of 5km along profile 1 in the Ethiopian rift.

B. The controlled seismic source is power gel C^+ with premix booster and explosive cords, and the recording seismic device is Guralp 6 TD recorder (band width 30s to 100Hz) picking the seismic impulse.

C. High resolution Gps were used for locating the Gurlap 6TDrecorder and shot point position and elevation. The Topographic map scale 1:50,000m were used during the Guralp 6TD recorder deployment recovery.

D. During estimation of ground particle vibration appropriate data processing and interpretation techniques have been used.

CHAPTER-4

4.1 Data Acquisition and Processing

The data required for this study were obtained from the controlled source seismic survey conducted as part of the Ethiopia Afar Geoscientific Lithospheric Experiment(EAGLE) in January 2003. The data acquisition of the EAGLE (controlled source survey) consists of three profile; the first profile,across the rift through Boset magmatic segment extending from the Blue Nile gorge in the North west and to Ginir (in Bale region) in the south east;the second profile , an axial profile extending from Awass in the south to Gewane in the North and the third profile, a central areal array centered on the Boset magmatic segment.
This paper will focus on the part of 400km long cross rift profile to compare the peak particle velocity of the ground with the semi-empirical Oriard formula.

Fig 5 EAGLE Cross Rift Profile

Along the controlled source cross rift profile of EAGLE project; 97 Guralp 6TD recorders (band width 30s to 100hz) were deployed at a nominal spacing of 5km, one month before the controlled source project took place. The other 339 are Reftek Texans single channel recorders (using 4.5Hz geophones) deployed at a nominal 1km spacing and buried approximately 15cm deep.

From the seismic instruments deployed across the rift only the data recorded by Guralp 6TD recorders have been used for the selection of the best recorded trace. The location and elevation of these relatively best-recorded geophones along the study are summarized in Table1.

Table 1 Shows the location and elevation of the relatively best recorded geophones used in the study

Site	Easting	Northing	Zone	Elevation (M)
11 51	513096.1	996815.7	37	2484
1155	513574.5	992716.8	37	2403
11 57	514208.8	991094.8	37	2378
11 63	516065.3	986922.4	37	2309
11 71	525836.7	984527.6	37	2356
11 79	526760.4	977479.6	37	2415
11 82	527905.9	974571.6	37	2377
12 04	543958.1	961313.9	37	1536
12 09	547001.2	956665.5	37	1460
12 19	549953.6	948247.8	37	1870
12 26	522660.2	942597.5	37	1817
12 31	550843.5	938088.5	37	1479
12 35	522982.9	936423.1	37	1453
12 42	559319.7	938980.3	37	1316
12 46	562679.2	939835.0	37	1266
12 52	565139.8	934688.0	37	1325
15 58	569545.0	930325.2	37	1803
12 62	572261.1	927201.8	37	2087
12 66	573883.6	924316.9	37	2170
1274	572538.3	915689.5	37	2606
1278	575870.8	914139.1	37	2646

Site	Easting	Northing	Zone	Elevation (M)
12 81	576406.4	911657.7	37	2708
12 85	576782.6	907614.1	37	2686
12 90	579066.1	903780.9	37	2687
12 96	578826.5	898225.6	37	2816
13 05	575746.9	890436.0	37	2568
13 15	575824.4	881534.0	37	2478
13 29	586371.7	873281.7	37	2477
13 37	592024.6	867683.8	37	2489

From a total of 19 bore hole shots fired by the EAGLE only 3 shots were used in this study. The selected bore hole EAGLE shot points found at Chefedonsa ,Doni and Kula.

The bore holes were drilled using an air rotary system through the over burden and down the hole hammer (DTH) to the bottom with a minimum depth of 50m and diameter of 10.

The explosive type used for the study was power gel C^+ per 50m hole with primex booster and explosive chord.

SHOT HOLE DATA

Table-2 shot hole location of depth

No	Site Name	Identification No	Location			Elevation (m)	Depth	Water level (m)
			Easting	Northing	Zone			
1	Chefedonsa	Sp_{14}	513296	992641	37P	2368	51.60	Nil
2	Doni I	Sp_{15}	562849	942509	37P	1226	55	18.95
3	Kula	Sp_{16}	575823	886441	3P	2502	50	33.40

Table-3 shot time and charge size

No	Site Name	Identification No	Shot date	Shot Time (GMT)	Timer used	Size kg
1	Chefedonsa	Sp_{14}	12Jan/03	21:03:00	Gps/Leics	375
2	Doni	Sp_{15}	12 Jan/03	22:50:00	Elpaso	50
3	Doni B	Sp_{25}	12 Jan/03	21:50:00	Elpaso	1025
4	kula	Sp_{16}	13 Jan/03	21:10:00	Usgs	1100

The map shown below shows the shot point location and the profile line of the study area.

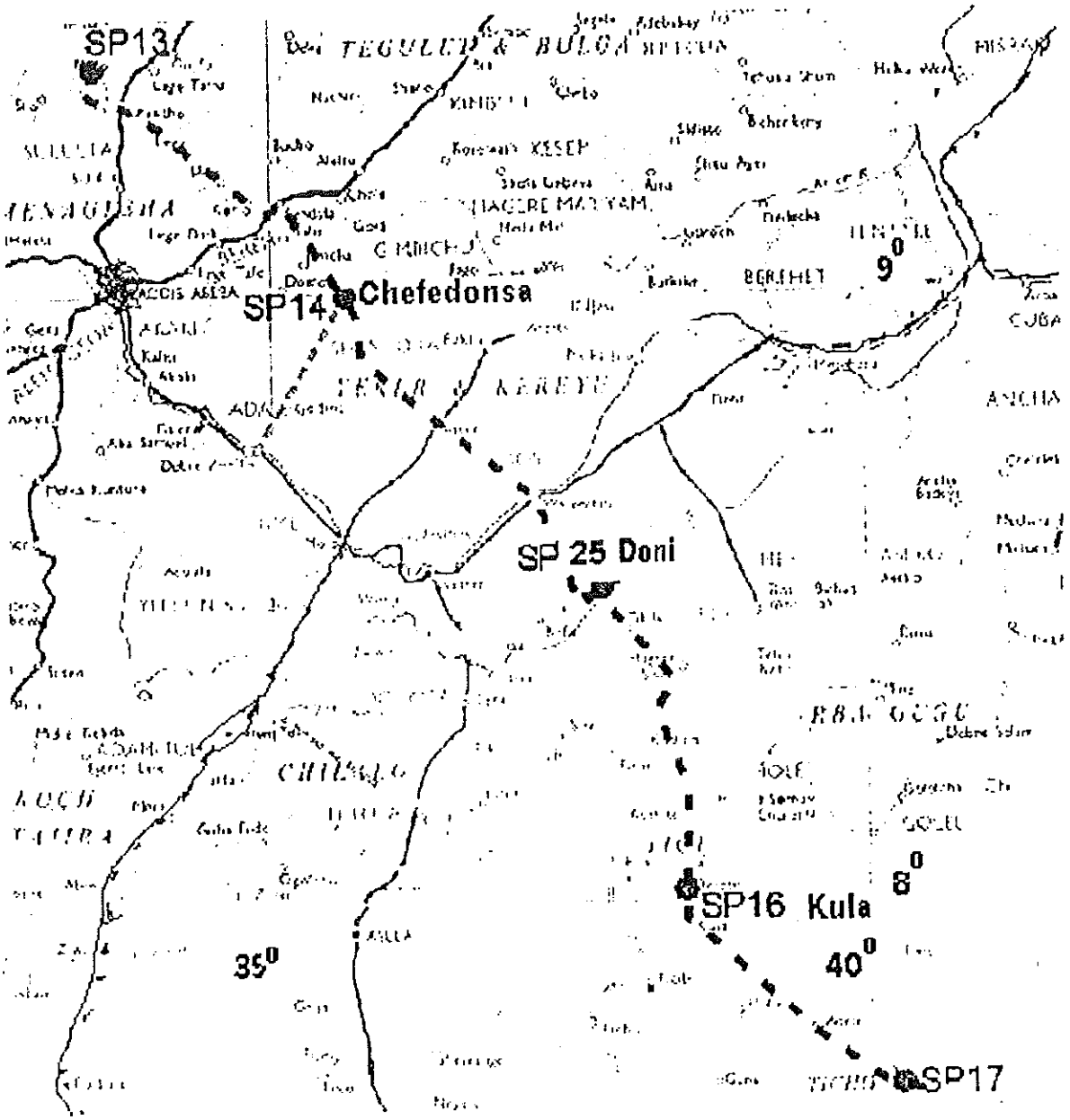

Fig.6 Map Showing the shot points and Guralp profile

Prior to each shot, the distance between shots and the nearest structure-usually unreinforced mud and wood house occasionally concret irrigation ditances or bridges were measured. Semi-empirical formulae derived from mining blasts by Hendron and Oriard (1972) were then used to calculate the likely bounds on the ground velocities at these structures and an appropriate chare size was selected to keep the predicted velocity of these structures below 2 inches/second (5cm/s), the threshold for cosmic damage recognized in the United States.
The recognized threshold for structural damage is 20 inches/second (50cm/s).

4.2 DATA PROCESSING

The seismic signals were sensed by the geophones and recorded by the Guralp 6TD recorder. The Guralp 6TD recorder can be used for registering a wide range of signals. The dynamic range (the range between the strongest and the weakest signals that can be recorded with out distortion by a given instrument) extends from very low frequency of 30s to high frequency of 100Hz.

The 6TD broadband seismometer converts the seismic signal in to a time record of seismic event (seismogram). The seismogram obtained from recorders represents a velocity recorded as a function of time.

The seismic signal recorded by the Guralp 6TD recorder has been analyzed and seismic wave identification performed for each geophone. Some Appropriate time window was selected to pick surface wave induced peak particle velocity of the ground. To emphasize the surface wave signals and help easy determination of the signal strength selected in the appropriate time window a filter bp bu co 0.8 2np 2p 2 was used.

To obtain a numerical value for the PPV from the surface wave selected in the appropriate time window we use a computer program known as SAC. The peak particle velocity data obtained from the seismograph of the selected geophones

according to their shot distance, shot size and shot site environment using the above process were given in the tables below.

Table – 4 Observed pick particle velocities data shot point site environmental -Chefedonsa (Shot size 375 kg)

No	Site	Distance (km)	Amplitude(cm/s)	Confinement Factor
1	1157	1.79	$2.3 X10^{5}$	$2 X10^{-2}$
2	1163	6.35	$4.53 X10^{3}$	$4.53 X10^{-4}$
3	1171	14.9	$2.7 X10^{3}$	$2.7 X10^{-4}$
4	1179	20.3	$2.5 X10^{3}$	$2.7 X10^{-4}$
5	1182	23.2	$1.8 X10^{3}$	$1.8 X10^{-4}$
6	1204	43.9	$1.6 X10^{3}$	$1.6 X10^{-4}$
7				
8	1219	57.6	$1.96 X10^{3}$	$1.96 X10^{-4}$
9	1226	63.7	$1.2 X10^{3}$	$1.2 X10^{-4}$
10	1231	66.2	$1.88 X10^{3}$	$1.88 X10^{-4}$
11	1235	68.8	$1.98X10^{3}$	$1.98X10^{-4}$
12				
13	1242	70.7	$9.7 X10^{2}$	$9.7 X10^{-4}$
14	1246	72.3	$1.43 X10^{3}$	$1.43 X10^{-4}$
15	1258	84	$1.3 X10^{3}$	$1.3 X10^{-4}$
16	1262	88.1	$1.44 X10^{3}$	$1.44 X10^{-4}$
17	1266	91.4	$1.42 X10^{3}$	$1.42 X10^{-4}$
18	1274	97.1	$1.6 X10^{3}$	$1.6 X10^{-4}$
19	1278	100.4	$1.2 X10^{3}$	$1.2 X10^{-4}$
20	1281	102.7	$1.5 X10^{3}$	$1.5 X10^{-4}$
21	1290	110.6	$1.57 X10^{3}$	$1.57 X10^{-4}$
22	1315	127.5	$1.4 X10^{3}$	$1.4 X10^{-4}$
23	1324	135	$1.33 X10^{3}$	$1.33 X10^{-4}$
24	1329	140	$1.48 X10^{3}$	$1.48 X10^{-4}$
25	1337	147.7	$1.33 X10^{3}$	$1.33 X10^{-4}$

Table 5 Shot Point Site-Doni A (Shot Size 50 kg)

Site	Distance (km)	Ampliitude (ηm/s)	Oriard min V (cm/s))	Oriard max V (cm/s)
1246	2.68	0.000992	2.65856	
1252	8.15	0.000184	1.4996	
1258	13.9	0.000145	2.0155	
1262	17.98	0.000126	2.26548	
1266	21.3	0.000096	2.0448	
1274	28.5	0.000104	2.964	
1278	31.2	0.000101	3.1512	
1281	33.7	0.000128	4.3136	
1285	37.6	0.000066	2.49664	
1290	42	0.000133	5.586	
1296	47.1	0.000129	6.0759	
1301	49.5	0.000099	4.9005	
1151	73.7	0.000160	11.792	
1155	70.4	0.000164	11.5456	
1157	68.8	0.000199	13.6912	
1171	56	0.000224	12.544	
1179	50.3	0.000152	7.6456	
1182	47.4	0.000132	6.2568	
1204	26.7	0.000180	4.806	
1209	21.3	0.000204	4.3452	
1219	14.1	0.000154	2.1714	
1226	10.2	0.000154	1.5708	

Table 6 Observed Pick Particle Velocities data shot Point

Site Environment-Kula (Shot Size 1100 kg)

Site	Distance (km)	SD	Vob	Oriard min V (cm/s))	Oriard max V (cm/s)
1182	104	3135.718	0.000123	0.0000825	0.0007590
1204	81.4	2454.302	0.000166	0.0001200	0.0011100
1209	75.9	2288.471	0.00031	0.0001340	0.0012300
1219	67	2020.126	0.000168	0.0001620	0.0014900
1226	60.8	1833.189	0.00017	0.0001890	0.0017400
1231	57.4	1730.675	0.000172	0.0002060	0.0019000
1235	55	1658.312	0.000145	0.0002200	0.0021000
1242	55.1	1661.328	0.000102	0.0002200	0.0021000
1246	55	1658.312		0.0002200	0.0021000
1252	49.4	1489.466	0.00015	0.0002600	0.0023900
1258	44.4	1338.71	0.000157	0.0003060	0.0028200
1262	40.9	1233.181	0.000158	0.0003470	0.0032000
1266	37.9	1142.728	0.000135	0.0003900	0.0035900
1274	29.5	889.4585	0.000177	0.0005750	0.0052900
1278	27.5	829.1562	0.00015	0.0006400	0.0058900
1281	25.2	759.8086	0.000133	0.0007320	0.0067400
1285	21.2	639.2041	0.000268	0.0009560	0.0087900
1290	17.7	533.6751	0.000634	0.0012600	0.0011600
1296	12.2	367.8438	0.000967	0.0022400	0.0026000
1301	8.4	253.2695	0.0015	0.0039800	0.0036600

Table – 7 Scaled distance V min, V max and observed pick particle velocities and confinement factor for Chefe Donsa shot point site (Shot size = 375kg)

Site	Scaled distance ($km/kg^{1/2}$)	observed amplitude(cm/s)	V min cm/s	V max cm/s	Confinement Factor
1157	92.4	$2.3 X10^{-2}$	$1.9 X 10^{-2}$	$1.73 X 10^{-1}$	24.45
1163	327.9	$4.53 X10^{-4}$	$2.67 X 10^{-2}$	$2.45 X 10^{-2}$	3.39
1171	769.4	$2.7 X10^{-4}$	$7.18 X 10^{-4}$	$6.61 X 10^{-3}$	7.52
1179	1048.3	$2.5 X10^{-4}$	$4.46 X 10^{-4}$	$4.10 X 10^{-3}$	11.2
1182	1198.1	$1.8 X10^{-4}$	$3.63 X 10^{-4}$	$3.34 X 10^{-3}$	9.9
1204	2267	$1.6 X10^{-4}$	$1.36 X 10^{-4}$	$1.25 X 10^{-3}$	23.5
1219	2974.5	$1.96 X10^{-4}$	$1.0 X 10^{-4}$	$8.2 X 10^{-4}$	43.8
1226	3289.5	$1.2 X10^{-4}$	$7.67 X 10^{-5}$	$7.1 X 10^{-4}$	31.3
1231	3418.6	$1.88 X10^{-4}$	$7.23 X 10^{-5}$	$6.65 X 10^{-4}$	52.03
1235	3552.8	$1.98X10^{-4}$	$6.81 X 10^{-5}$	$6.27 X 10^{-4}$	58.7
1242	3650.9	$9.7 X10^{-5}$	$6.5 X 10^{-5}$	$6.0 X 10^{-4}$	29.7
1246	2733.6	$1.43 X10^{-4}$	$6.3 X 10^{-5}$	$5.8 X 10^{-4}$	45.3
1258	4337.7	$1.3 X10^{-4}$	$5 X 10^{-5}$	$4.6 X 10^{-4}$	51.91
1262	4549.5	$1.44 X10^{-4}$	$4.6 X 10^{-5}$	$4.3 X 10^{-4}$	61.9
1266	4719.9	$1.42 X10^{-4}$	$4.39 X 10^{-5}$	$4.0 X 10^{-4}$	64.59
1274	5014.2	$1.6 X10^{-4}$	$4.0 X 10^{-5}$	$3.68 X 10^{-4}$	79.9
1278	5184.6	$1.2 X10^{-4}$	$3.8 X 10^{-5}$	$3.5 X 10^{-4}$	63.1
1281	5303.4	$1.5 X10^{-4}$	$3.7 X 10^{-5}$	$1.3 X 10^{-4}$	81.7
1290	5711.4	$1.57 X10^{-4}$	$3.28 X 10^{-5}$	$3.02 X 10^{-4}$	95.8
1215	6584.1	$1.4 X10^{-4}$	$2.63 X 10^{-5}$	$2.42 X 10^{-4}$	106.3
1324	6971.4	$1.33 X10^{-4}$	$2.4 X 10^{-5}$	$2.2 X 10^{-4}$	110.3
1329	7229.6	$1.48 X10^{-4}$	$2.3 X 10^{-5}$	$2.1 X 10^{-4}$	129.8
1337	7591	$1.33 X10^{-4}$	$2.1 X 10^{-5}$	$1.95 X 10^{-4}$	125.75

Table – 8 Scaled distance V min, V ma and observed pick particle velocities and confinement factor for Doni shot point site (Shot size = 50kg)

Site	Scaled distance (m/kg1/2)	observed amplitude(cm/s)	V min cm/s	V max cm/s	Confinement Factor
1246	379.0	9.92×10^{-4}	2.63×10^{-3}	1.96×10^{-2}	9.28
1252	1203.5	1.84×10^{-4}	3.61×10^{-4}	3.32×10^{-3}	10.2
1258	1965.8	1.45×10^{-4}	1.69×10^{-4}	1.56×10^{-3}	17.12
1262	2542.8	1.26×10^{-4}	1.14×10^{-4}	1.05×10^{-3}	22.10
1266	3012.3	9.6×10^{-5}	8.78×10^{-5}	8.08×10^{-4}	28.91
1274	4030.5	1.04×10^{-4}	5.61×10^{-5}	5.16×10^{-4}	37.1
1278	4412.3	1.01×10^{-4}	4.88×10^{-5}	4.49×10^{-4}	41.4
1281	4765.9	1.28×10^{-4}	4.33×10^{-5}	3.99×10^{-4}	59.1
1285	5317.4	6.64×10^{-5}	3.66×10^{-5}	3.37×10^{-4}	36.3
1290	5939.7	1.33×10^{-4}	3.1×10^{-5}	2.84×10^{-4}	86.2
1296	6660.9	1.29×10^{-4}	2.59×10^{-5}	2.38×10^{-4}	99.7
1301	7000.4	9.9×10^{-5}	2.39×10^{-5}	2.20×10^{-4}	82.6
1151	10422.8	1.6×10^{-4}	1.3×10^{-5}	1.19×10^{-4}	246.5
1155	9956.6	1.64×10^{-4}	1.39×10^{-5}	1.2×10^{-4}	235.5
1157	9726.8	1.99×10^{-4}	1.44×10^{-5}	1.3×10^{-4}	275.8
1171	7919.3	2.4×10^{-4}	1.98×10^{-5}	1.8×10^{-4}	226.07
1179	7113.5	1.52×10^{-4}	2.34×10^{-5}	2.15×10^{-4}	130.03
1182	6703.4	1.32×10^{-4}	2.56×10^{-5}	2.34×10^{-4}	42.58
1204	3775.95	1.8×10^{-4}	6.2×10^{-5}	5.7×10^{-4}	58.06
1209	3012.3	2.04×10^{-4}	8.78×10^{-5}	8.1×10^{-4}	46.50
1219	1994.04	1.54×10^{-4}	1.66×10^{-5}	1.52×10^{-4}	18.6
1226	1442.5	1.54×10^{-4}	2.73×10^{-5}	2.51×10^{-4}	11.28

4.2.1 Ground Vibration

The peak particle velocity prediation across the rift can be made using the semi- emperical oriard formula. using orlard

Maximum predicted Velocity = Vmax (cm/s) = 154[off set] charge wt ½ -1-54 kg

Minimum predicted Velocity = Vmin (cm/s=20 [offe set] (charge wt /kg $)^{1/2}$] – 1.54 kg

using the scaled distance for the selected geophones of each shot pint environment, the observed pick particle velocity, vmin and Vmax were given in the following table

The figure below shows the graph of Vmax, Vmin and persion of the observed velocity on the log velocity/ log-scaled distance.

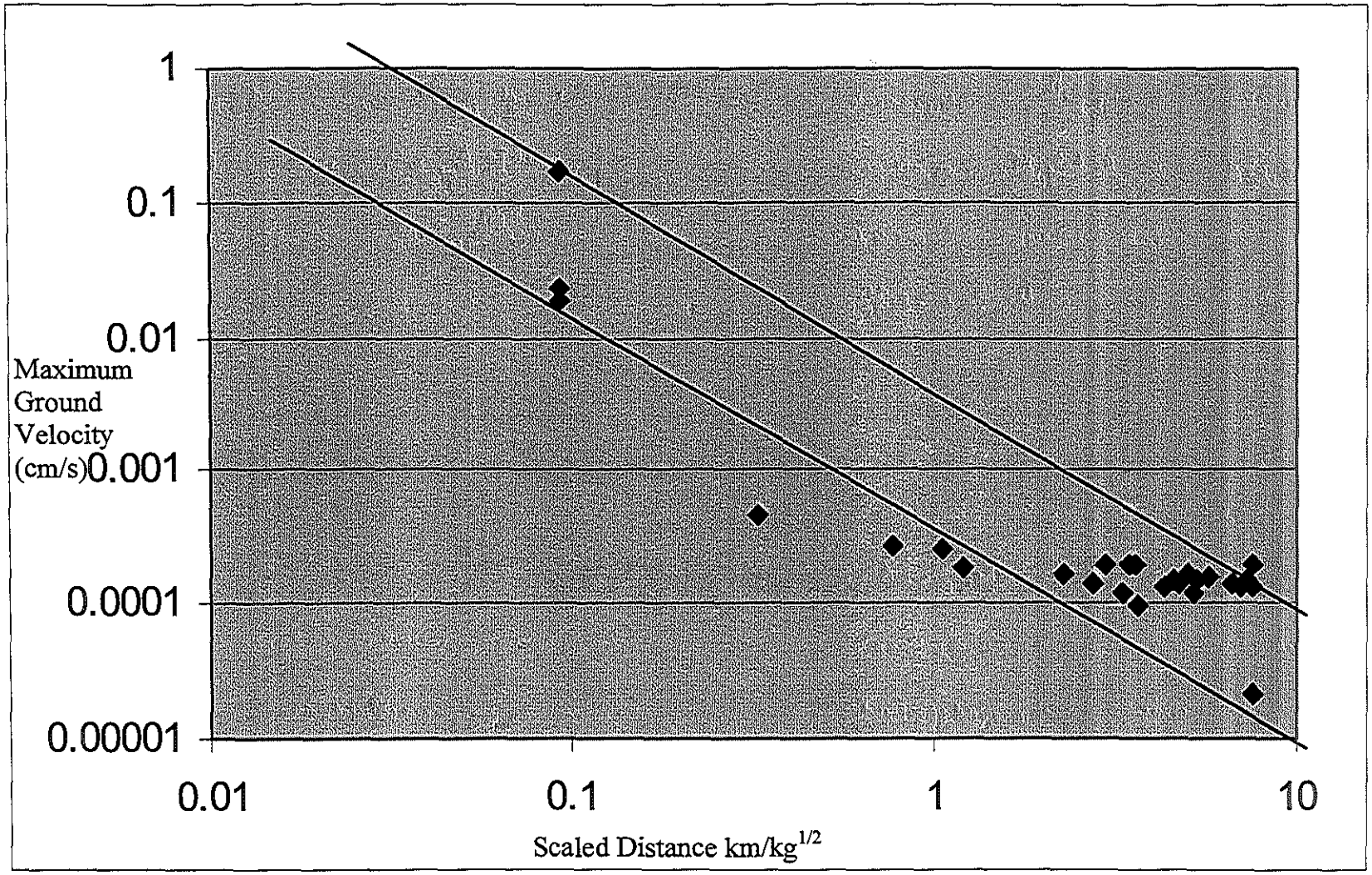

Fig 7 Graph of maximum ground velocity against scaled distance for Chefe-Donsa

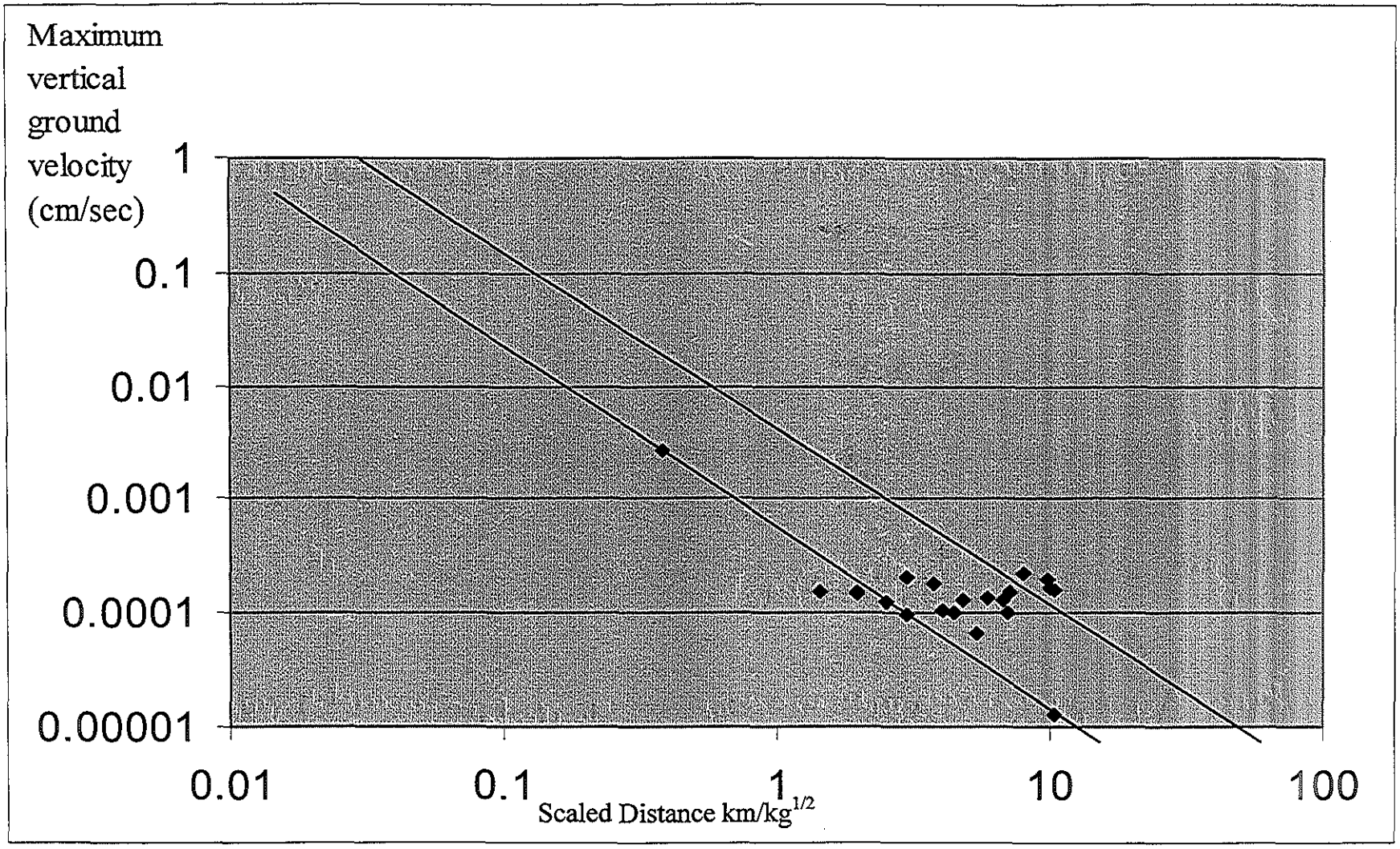

Fig 8 Graph of maximum ground velocity against scaled distance for Doni

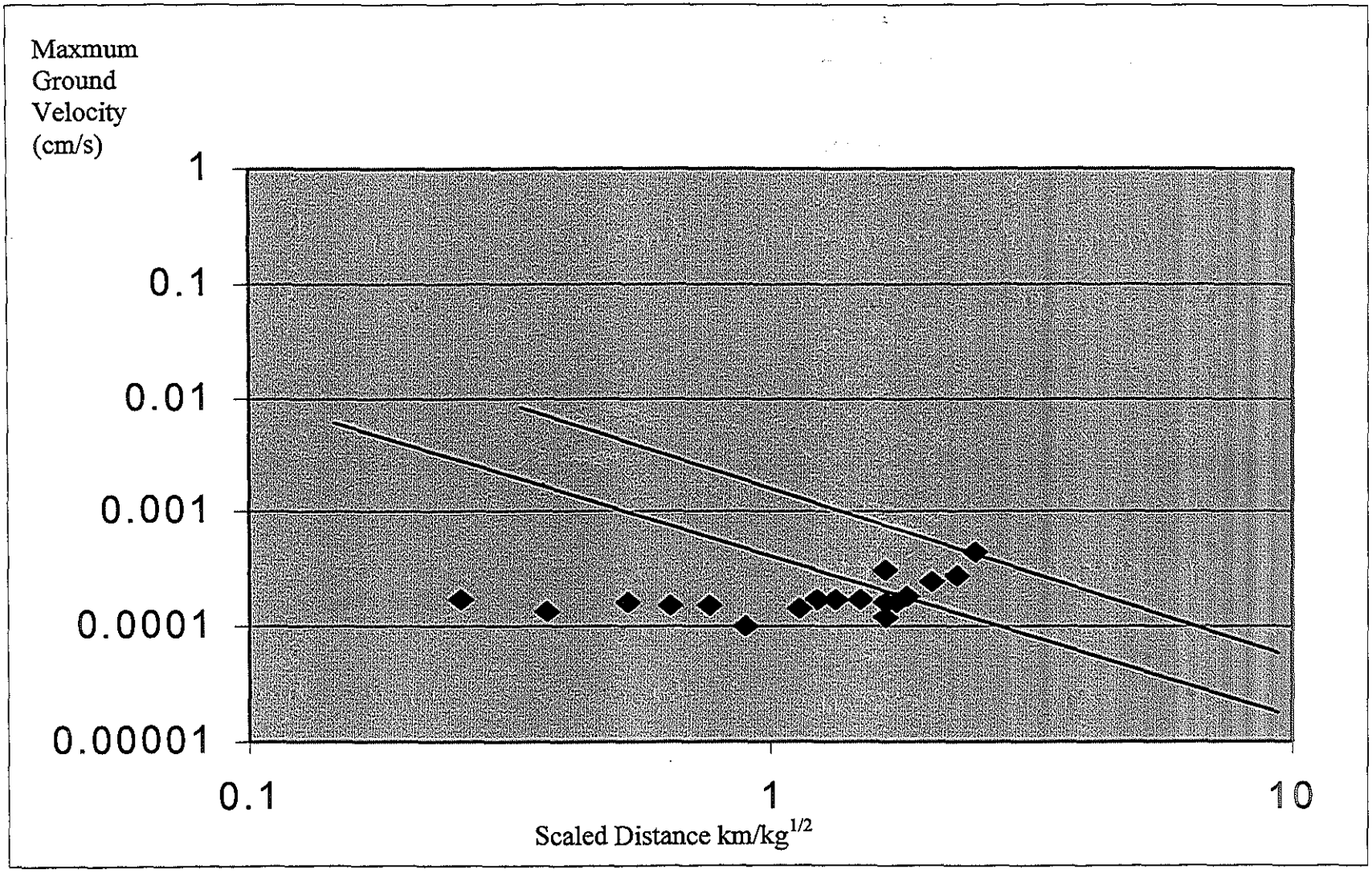

Fig 9 Graph of maximum ground velocity against scaled distance for Kula

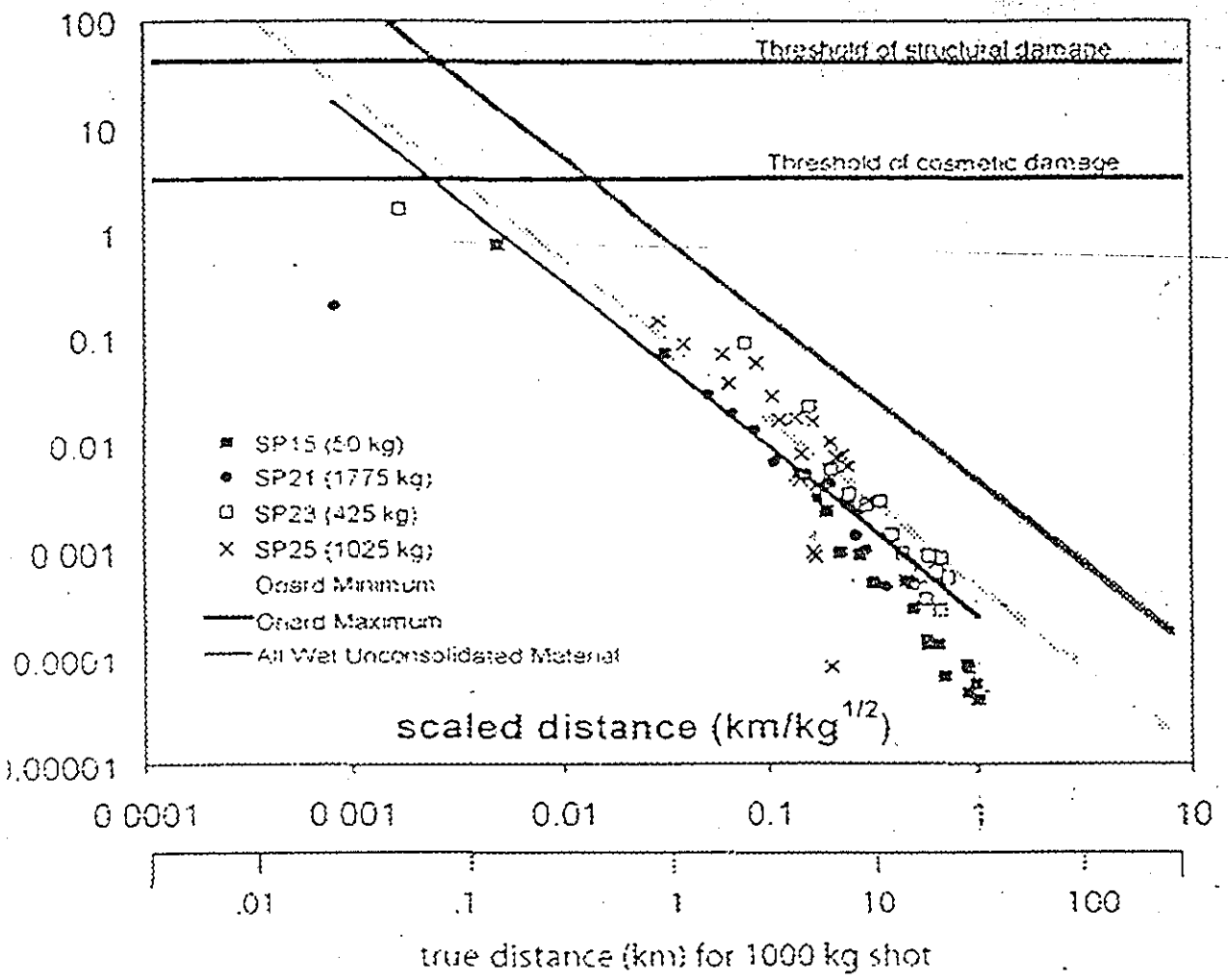

Fig 10 Graph of maximum ground velocity against scaled distance for bore hole shot in wet unconsolidated material

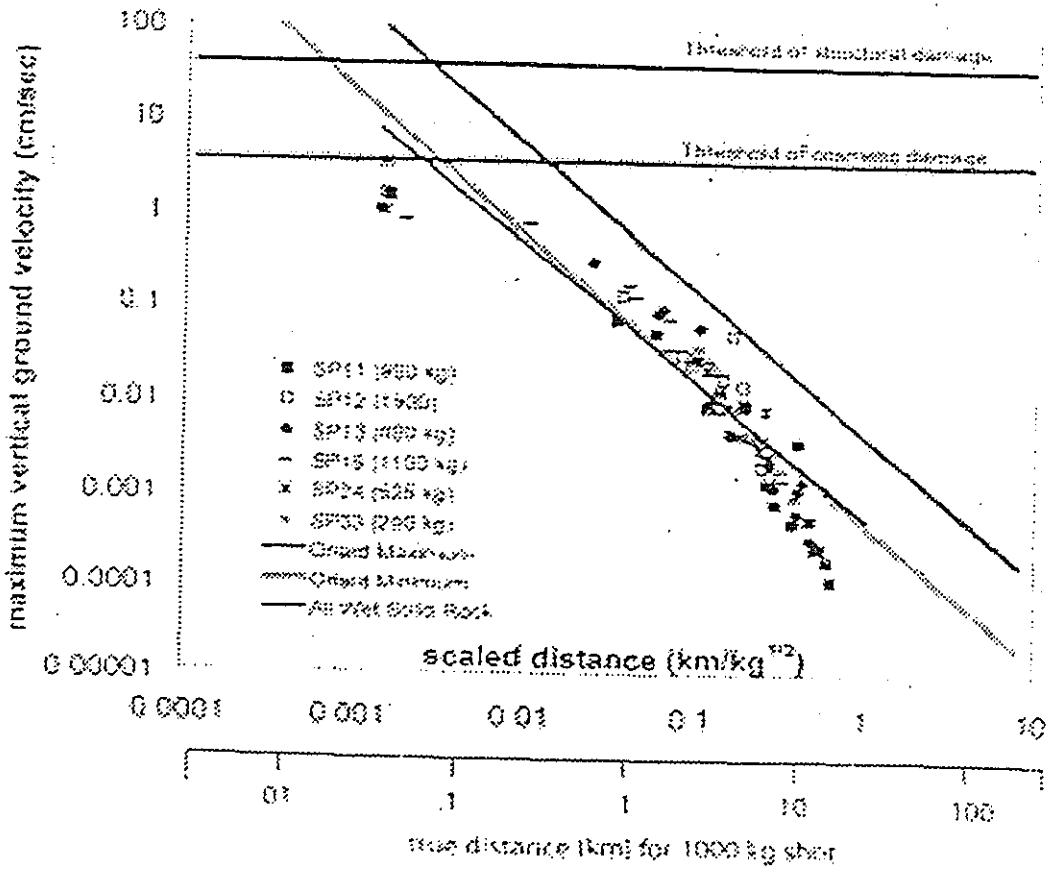

Fig 11 Graph of maximum ground velocity against scaled distance for bore hole shot in wet solid rock

CHAPTER 5

5.1 Results and Interpretation

Based on scaled distance, shot point site environment the outcome of the research in comparison to Oriard prediction and the results of the study analyzed by Stanford University be presented as follows.

The Oriard formula predicts maximum ground velocities well for relatively lower velocities at greater than 1.85 km per kg1/2 for both SP14 and SP16 represent for Chefe-Donsa and Kula respectively. While for SP15 that represents Doni shot point site environment predicts well at relatively intermediate velocities from 2-8 km per kg1/2scaled distance. However, the Oriard over predicts maximum ground velocity for higher velocities pertinently for scaled distance approximately less than 1.85 km per kg1/2for both SP14 and SP16. The Oriard over predicts for relatively higher velocities scaled distance less than 2 km per kg1/2, while in contrary under predicts for relatively lower velocities at scaled distance greater than 8 km per kg1/2 to that of SP15. The EAGLE data from SP15 and SP16 for scaled distance between 0.01 and 10 km per kg1/2 shows concave upward due to a slow decrement of velocity of surface wave along the transect than that of Oriard with scaled distance. In addition, the result of the ground velocity compared to that of Stanford University Department of Geophysics, although for their study they analyze records at less than 1 km per kg1/2 scaled distance for each shots, nevertheless, we analyzed recording in the range 0.1-10 km per kg1/2 scaled distance. The comparison prompts for SP15 and SP16 demonstarted in fig 4 and fig 5 (EAGLE,2003 unpublished report perpendicular 123-124) and the comparison of the results are as follows:

Compared to the Stanford University results for SP15 and SP16 as indicated in fig 4 and fig 5 our result is well fitted with them in the range of scaled distance 0.1-1 km per kg1/2.

5.2 Conclusion

Eventbually, the comparisons have an excite points that asserts the consistency of the deduction with the Stanford University Department of Geophysics, once further more accurate prediction of velocities at these small offsets would permit the use of large shot sizes without increased risk to structures.

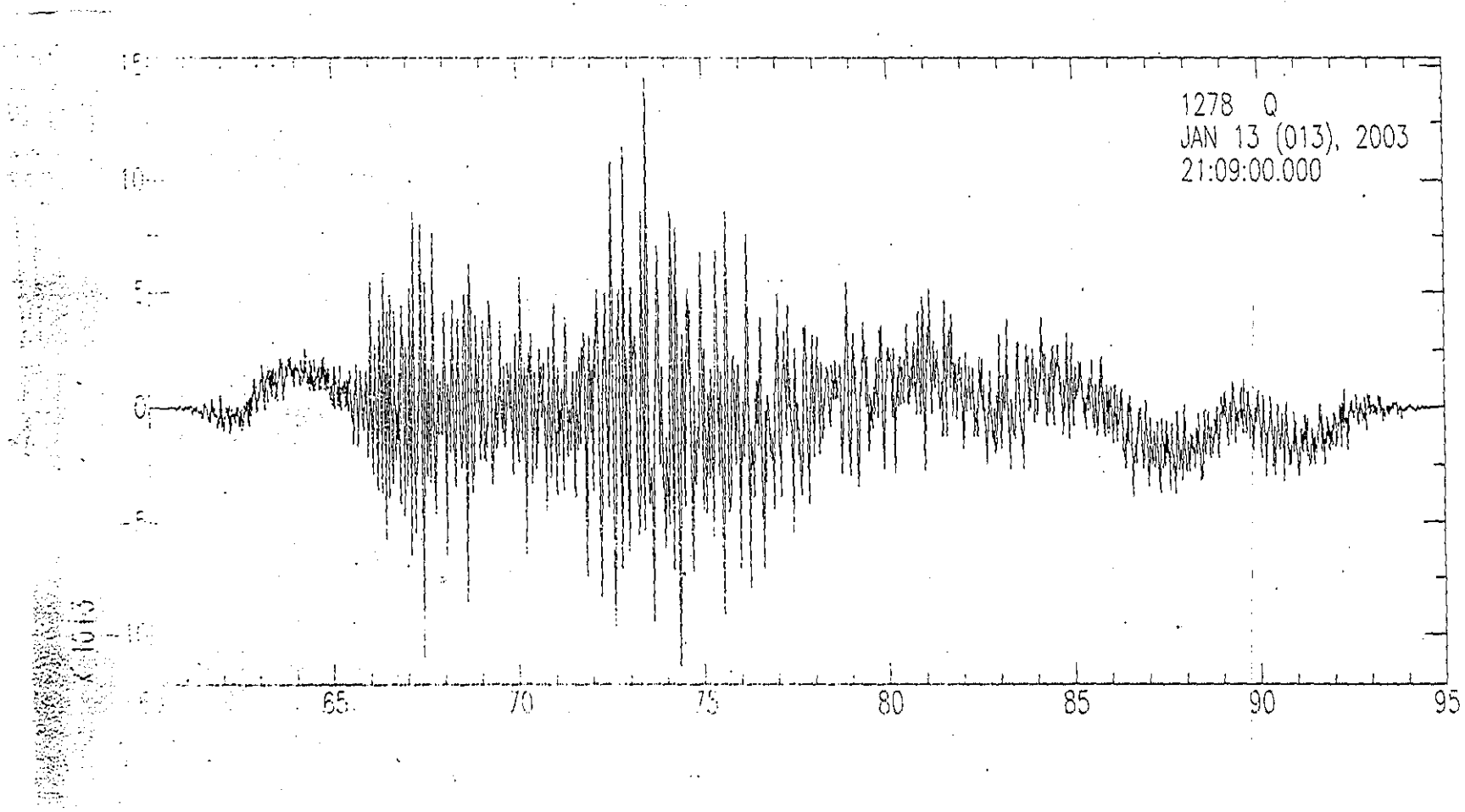

Fig 12 Seismic record for SP14

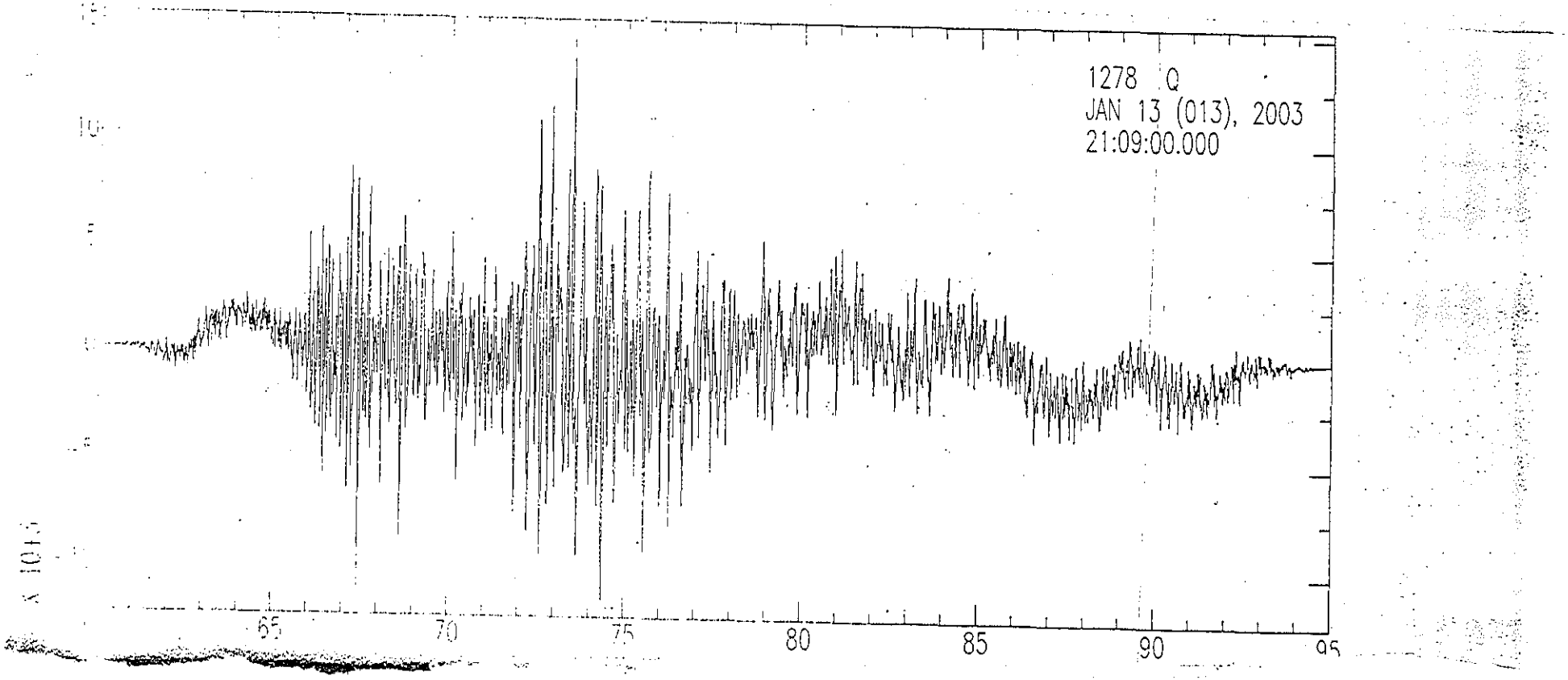

Fig 13 Seismic record for SP16

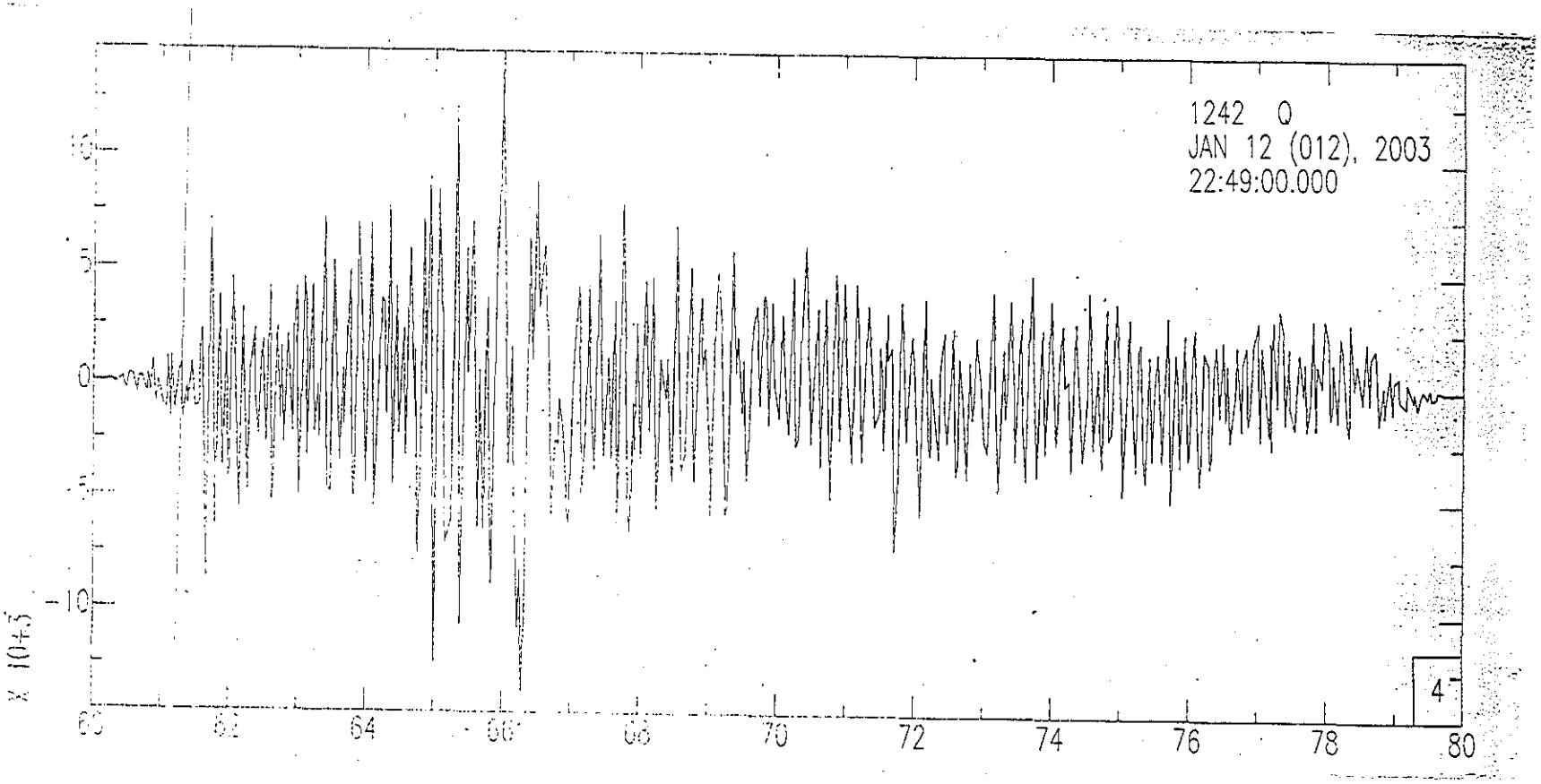

Fig 14 Seismic wave for relatively good geophone- SP14

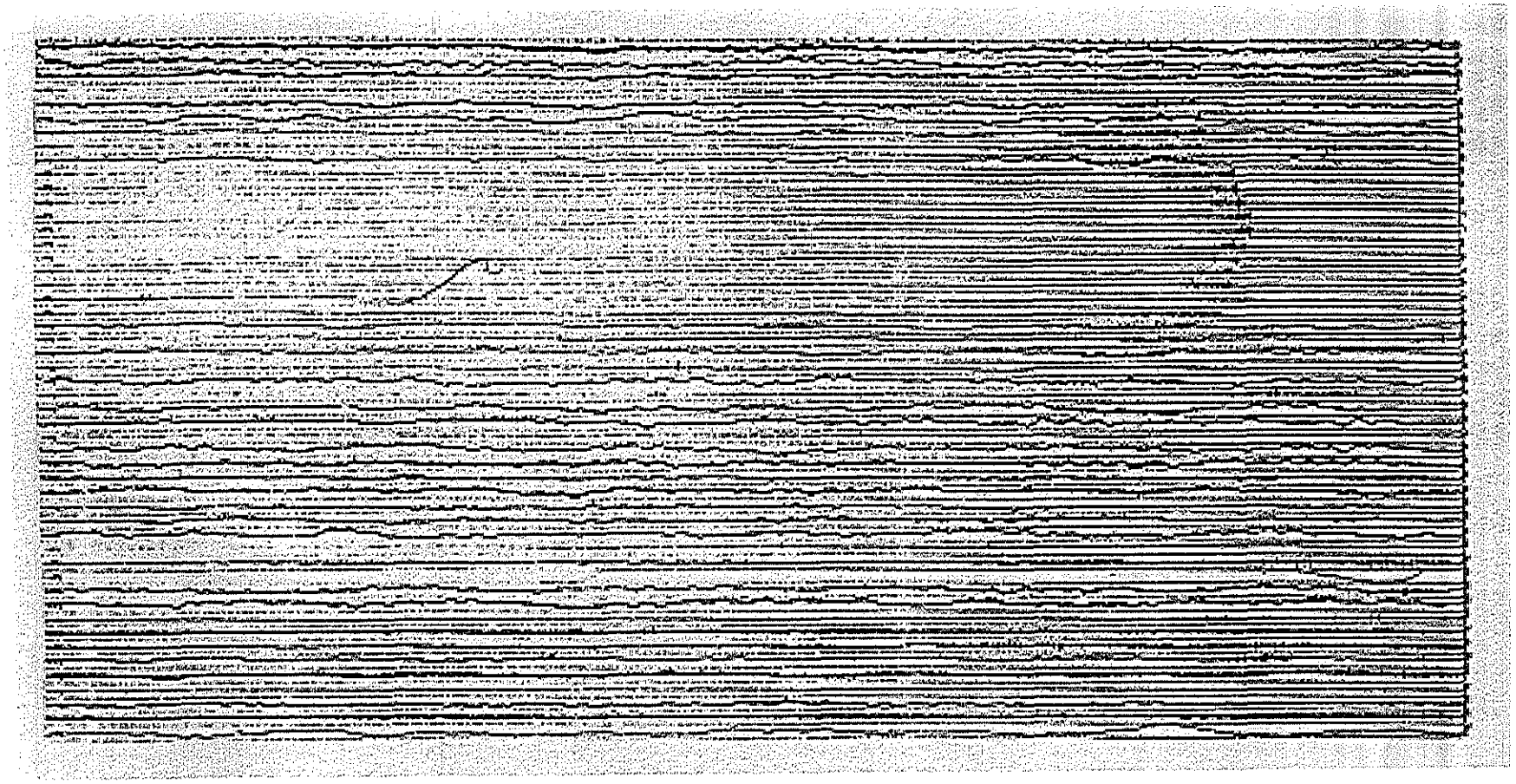

Fig 15 Seismic wave for relatively good geophone- SP15

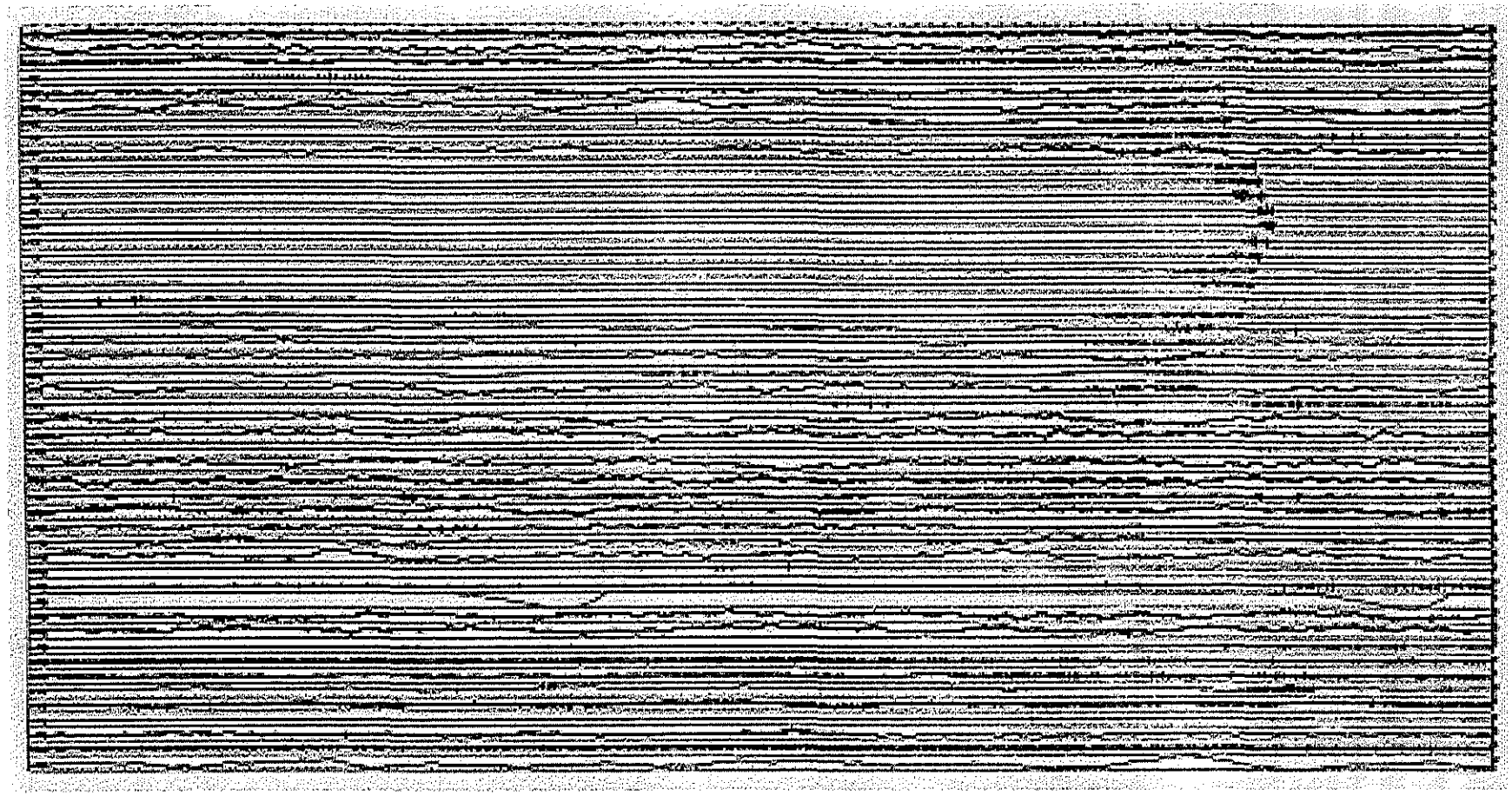

Fig 16 Seismic wave for relatively good geophone- SP16

References

1. Mazzarini 1999
2. Zanetti and Justin,1994
3. Ritcher, 1957
4. Hendron and Oriard ,1972